



A Study of Small Perturbations in the Coriolis And Centrifugal Forces in RR3BP with Finite Straight Segment

¹Bhavneet Kaur, ^{2*}Dinesh Kumar and ³Shipra Chauhan

¹Department of Mathematics
Lady Shri Ram College for Women
University of Delhi
Delhi, India
bhavneet.lsr@gmail.com

^{2,3}Department of Mathematics
University of Delhi
Delhi, India
²dineshk8392@gmail.com
³chauhanshipra10@gmail.com

*Corresponding Author

Received: January 14, 2020; Accepted: April 27, 2020

Abstract

In this paper, the effect of small perturbations in the Coriolis and centrifugal forces on the existence and stability of the equilibrium point in the Robe's restricted three-body problem (RR3BP) by taking the smaller primary as a finite straight segment is introduced. In the present structure the density ρ_1 of the fluid filled in the bigger primary of mass m_1^* and the density ρ_3 of the infinitesimal body of mass m_3 are considered to be equal. It is worth mentioning that the location of the equilibrium point is affected by a small perturbation in the centrifugal force. The present model possesses one equilibrium point L_1 which is collinear with the center of mass of the primaries. It lies towards the right or left of the center of the shell according as the perturbation π_2 in the centrifugal force is positive or negative. Further, the stability of L_1 is analyzed. The range of stability is affected not only by the perturbations in the Coriolis and centrifugal forces but also by the length of the finite straight segment. For $0 < \mu \leq \mu^*$, L_1 is unstable whereas for $\mu^* < \mu < 1$ it becomes stable. It is observed that the Coriolis force is a stabilizing force provided the centrifugal force is kept constant while the centrifugal force is a destabilizing force when the Coriolis force is kept constant.

Keywords: Robe's restricted three-body problem; Coriolis force; Centrifugal force; Finite straight segment

MSC 2010 No.: 37N05, 70F07, 70F15

1. Introduction

The three-body problem is one of the most significant and most popularly research problem in celestial mechanics having its applications ranging from astrodynamics, astrophysics, cosmology and stellar dynamics to name a few. The problem attracts the attention of several researchers who have done pioneer work analytically and numerically by considering various modifications of the dynamical model. The general three-body problem focusses on the motion of three bodies moving under their mutual gravitational attraction, whereas the restricted problem emphasizes on the motion of the infinitesimal body whose mass is negligible in comparison to the masses of the other two primary bodies.

Robe (1977) permuted the restricted three-body problem by taking the shape of the massive primary as a rigid spherical shell in contrast to a point mass. The practicality of the dynamical setup is in the study of the small oscillations of the Earth's inner core due to the Moon's attraction. His analysis suggested that the center of the Earth is a stable position for the Earth's core. This remarkable contemplation of the RR3BP paved way for several researchers to follow his legacy. Plastino and Plastino (1995) revisited the Robe's problem by assuming the hydrostatic equilibrium figure of the first primary as Roche ellipsoid (Chandrasekhar (1987)). An extensive investigation has been done in this field henceforth by Giordano et al. (1997), Hallan and Rana (2001b), Singh and Sandah (2012), Singh and Omale (2014), and Singh and Mohammed (2012, 2013) to name a few.

In the series of papers, a significant extension of the Robe's problem to $2 + 2$ body problem has been done by Kaur and Aggarwal (2012, 2013a, 2013b), Aggarwal and Kaur (2014), and Aggarwal et al. (2018) by considering the variations in the shapes of the primaries as oblate and triaxial. A praiseworthy generalization of the Robe's problem has been done by Singh and Leke (2013). They investigated the linear stability of the equilibrium points of the infinitesimal mass in the framework of Robe's circular restricted three-body problem together with effect of variation in masses of the primaries with time according to the combined Meshcherskii law.

The perturbations refer to the departure of the dynamical system from an idealized setup. The resourcefulness of Szebehely (1967) in the investigation of the effect of a small perturbation in the Coriolis force by leaving the centrifugal effect undisturbed suggested that the collinear equilibrium points are always unstable. The range of stability of the non-collinear equilibrium points increase or decrease according to the change in the Coriolis force is positive or negative. He established that the Coriolis force is a stabilizing force. Motivated by the work done by Szebehely (1967), Subbarao and Sharma (1975) extended their work by considering one of the primaries as an oblate spheroid. They emphasized that the Coriolis force is not always a stabilizing force when the centrifugal force is not considered as a constant.

The work of Szebehely (1967) and Subbarao and Sharma (1975) was unfolded by Bhatnagar and Hallan (1978). They demonstrated that the range of stability of the non-collinear equilibrium points increase or decrease depending upon whether the point (π_1, π_2) lies in one or the other of the two parts in which the (π_1, π_2) plane is divided by the line $36\pi_1 - 19\pi_2 = 0$. The stability of the collinear equilibrium points are not influenced by the perturbations in the Coriolis and centrifugal

force and they remain unstable. Rigorous work on perturbations in the Robe's problem has been explored by Shrivastava and Garain (1991), Kaur et al. (2016), and Hallan and Mangang (2008) to cite a few.

Riaguas et al. (2001) studied the non-linear stability of the equilibrium points in the gravity field of the finite straight segment. Jain and Sinha (2014b, 2014a) explored the consequences on taking both the primaries as finite straight segments on the locations and stability of the equilibrium points and regions of motion in the linear and non-linear sense respectively. Revolutionary upgradation of the ideas of Robe (1977) and Riaguas et al. (2001) were compassed by Kumar et al. (2019). They investigated the existence and linear stability of the equilibrium points in the Robe-finite straight segment framework.

In the realm of the innumerable endeavors of the authors, we draw inspiration to review the location and stability of the equilibrium point in the Robe's circular problem by taking into account the effect of small perturbations in the Coriolis and centrifugal forces and the shape of the smaller primary as a finite straight segment. In this structure, we have speculated that the density ρ_1 of the incompressible fluid is same as that of the density ρ_3 of infinitesimal mass m_3 . The present analysis is very relevant considering that the several natural and artificial bodies are elongated.

The present paper is catalogued as follows. In Section 2, the description of the dynamical system and the equations of motion are presented. In the subsequent section, the existence of the equilibrium point and its evolution on varying parameters are inspected. In Section 4, the effect of varying parameters on the linear stability of the equilibrium point is conferred. Applications are included in Section 5. Finally, in Section 6, the conclusion of the problem is drawn emphasizing the correlation of our work with other authors.

2. Description of the dynamical system

In the present section, the effect of the small perturbations in the Coriolis and centrifugal forces on the configuration of the Robe's restricted three-body problem by taking the smaller primary as a finite straight segment is deliberated. The massive primary m_1^* is taken to be a rigid spherical shell filled with homogeneous incompressible fluid of density ρ_1 and the smaller primary a finite straight segment of mass m_2 and length $2l$ outside the shell. The problem is known as restricted since the third body of mass m_3 is a small solid sphere of density ρ_3 inside the shell and assumed to have an infinitesimal mass and radius. The motion of m_3 does not influence the motion of the primaries but it itself is influenced by them.

In addition, we consider that the density ρ_1 of the incompressible fluid is same as that of the density ρ_3 of m_3 , that is $\rho_1 = \rho_3$. The primary m_2 describes a circular orbit around m_1^* with constant angular velocity ω . The orbital plane of m_2 around m_1^* is taken as the (x, y) -plane and the origin of the coordinate system is at the center of mass O of the two finite bodies. It is assumed that the synodic system of coordinates which is initially coincident with the inertial system also rotate with angular velocity ω . We assume that the principal axes of m_2 is parallel to the synodic axes and their axes of symmetry be perpendicular to the plane of motion of the bodies. Since m_2

is revolving without rotation about m_1^* with the same angular velocity as that of the synodic axes, the principal axes of m_2 will remain parallel to them throughout the motion (Figure 1).

The gravitational force between m_1^* and m_2 is given by the following expression

$$F = G \frac{m_1^* m_2}{((b_1 + b_2)^2 - l^2)},$$

where G is the universal gravitational constant; b_1 and b_2 are the distances of m_1^* and m_2 , respectively, from the center of mass O .

Since m_2 is moving in circular orbit around m_1^* , therefore,

$$\omega^2(b_1 + b_2) = G(m_1^* + m_2) \left(\frac{1}{(b_1 + b_2)^2 - l^2} \right).$$

Further, we consider the units such that the sum of the masses of the primaries and the distance between them are 1 unit. The unit of time is chosen such that G becomes unity. Thus, on neglecting third and higher order terms of l , the expression of the mean motion is obtained as follows

$$\omega^2 = 1 + l^2, \text{ where } 0 < l \ll 1.$$

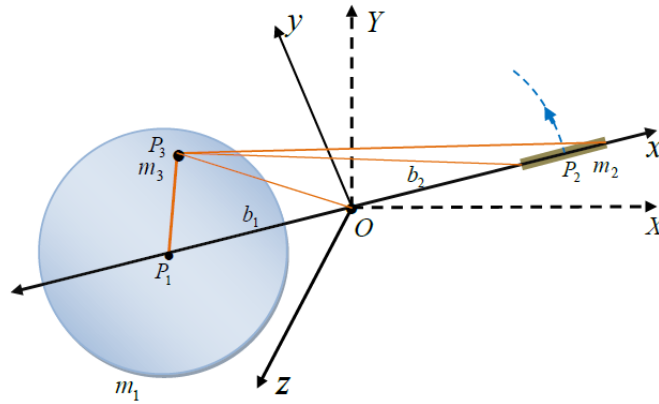


Figure 1. Configuration of the RR3BP in the synodic coordinate system

The dynamics of m_3 in non-dimensional synodic coordinate system is given by

$$\begin{aligned} \ddot{x} - 2\omega\dot{y} - \omega^2 x &= U_x, \\ \ddot{y} + 2\omega\dot{x} - \omega^2 y &= U_y, \\ \ddot{z} &= U_z, \end{aligned}$$

where

$$U(x, y, z) = \frac{\mu}{2l} \log \left(\frac{r_1 + r_2 + 2l}{r_1 + r_2 - 2l} \right),$$

$$\mu = \frac{m_2}{m_1^* + m_2}, \quad 0 < \mu < 1,$$

$$r_1^2 = (x - 1 + \mu + l)^2 + y^2 + z^2,$$

$$r_2^2 = (x - 1 + \mu - l)^2 + y^2 + z^2.$$

Here U_x , U_y and U_z represent the first order partial derivatives of $U(x, y, z)$ with respect to x , y and z , respectively.

Introducing the small perturbations in the Coriolis and centrifugal forces with the help of parameters $\alpha = 1 + \pi_1$, ($|\pi_1| \ll 1$) and $\beta = 1 + \pi_2$, ($|\pi_2| \ll 1$), respectively. The unperturbed values of α and β are unity. Consequently, the equations of motion are

$$\ddot{x} - 2\omega\alpha\dot{y} - \omega^2\beta x = U_x, \quad (1a)$$

$$\ddot{y} + 2\omega\alpha\dot{x} - \omega^2\beta y = U_y, \quad (1b)$$

$$\ddot{z} = U_z. \quad (1c)$$

The Equations (1a)-(1c) can be rewritten as

$$\ddot{x} - 2\omega\alpha\dot{y} = W_x, \quad (2a)$$

$$\ddot{y} + 2\omega\alpha\dot{x} = W_y, \quad (2b)$$

$$\ddot{z} = W_z, \quad (2c)$$

where

$$W(x, y, z) = \frac{1}{2}\omega^2\beta(x^2 + y^2) + \frac{\mu}{2l} \log \left(\frac{r_1 + r_2 + 2l}{r_1 + r_2 - 2l} \right),$$

and W_x , W_y and W_z are the first order partial derivatives of $W(x, y, z)$ with respect to x , y and z , respectively. If the length of the smaller primary is zero, Equations (2a)-(2c) coincide with Hallan and Rana (2001a). And when $\alpha = \beta = 1$, Equations (2a)-(2c) agree with Kumar et al. (2019) provided $k = 0$.

3. The location of the equilibrium point

The points at which the velocity and acceleration of m_3 are zero are called the equilibrium points. These points are the solutions of the equations

$$W_x(x, y, z) = W_y(x, y, z) = W_z(x, y, z) = 0.$$

Therefore, the coordinates of the equilibrium points can be retrieved by solving the following system of equations

$$\begin{aligned}\omega^2\beta x - \frac{2\mu}{[(r_1 + r_2)^2 - 4l^2]} \left(\frac{(x - 1 + \mu + l)}{r_1} + \frac{(x - 1 + \mu - l)}{r_2} \right) &= 0, \\ y \left[\omega^2\beta - \frac{2\mu}{[(r_1 + r_2)^2 - 4l^2]} \left(\frac{1}{r_1} + \frac{1}{r_2} \right) \right] &= 0, \\ z \left[\frac{2\mu}{[(r_1 + r_2)^2 - 4l^2]} \left(\frac{1}{r_1} + \frac{1}{r_2} \right) \right] &= 0,\end{aligned}$$

simultaneously. Therefore, the equilibrium points are the real solutions of the following system of equations

$$\omega^2\beta x - \frac{2\mu}{[(r_1 + r_2)^2 - 4l^2]} \left(\frac{(x - 1 + \mu + l)}{r_1} + \frac{(x - 1 + \mu - l)}{r_2} \right) = 0, \quad (3a)$$

$$y = 0, \quad (3b)$$

$$z = 0, \quad (3c)$$

and

$$\omega^2\beta x - \frac{2\mu}{[(r_1 + r_2)^2 - 4l^2]} \left(\frac{(x - 1 + \mu + l)}{r_1} + \frac{(x - 1 + \mu - l)}{r_2} \right) = 0, \quad (4a)$$

$$\omega^2\beta - \frac{2\mu}{[(r_1 + r_2)^2 - 4l^2]} \left(\frac{1}{r_1} + \frac{1}{r_2} \right) = 0, \quad (4b)$$

$$z = 0. \quad (4c)$$

The system of Equations (4a)-(4c) has no solution. The solution of Equations (3a)-(3c) correspond to the collinear equilibrium points lying on the x -axis. The abscissae of these points obtained by taking $y = z = 0$ are the solutions of the equation

$$\omega^2\beta x - \frac{2\mu}{[(r_1 + r_2)^2 - 4l^2]} \left(\frac{(x - 1 + \mu + l)}{r_1} + \frac{(x - 1 + \mu - l)}{r_2} \right) = 0, \quad (5)$$

where $r_1 = |x - 1 + \mu + l|$ and $r_2 = |x - 1 + \mu - l|$.

Since $x < 1 - \mu - l$, we have $r_1 = -(x - 1 + \mu + l)$ and $r_2 = -(x - 1 + \mu - l)$. Equation (5) can be recast into the following form by putting these values of r_1 and r_2 ,

$$(1 + l^2)\beta x + \frac{\mu}{[(x - 1 + \mu)^2 - l^2]} = 0. \quad (6)$$

For the sake of notational convenience, we denote the left hand side of the above equation by $f(x)$. The derivative of f with respect to x , denoted by f'

$$f'(x) = (1 + l^2)\beta - \frac{2\mu(x - 1 + \mu)}{[(x - 1 + \mu)^2 - l^2]^2},$$

is strictly positive for $x < 1 - \mu$. Since $l > 0$, therefore, $f'(x) > 0$ for $x < 1 - \mu - l$. We have the following observations for the function f

- (1) f is strictly increasing in $(-\infty, 1 - \mu - l)$,
- (2) $\lim_{x \rightarrow -\infty} f(x) = -\infty$,
- (3) $\lim_{x \rightarrow (1-\mu-l)} f(x) = +\infty$.

The above three points indicate that f becomes zero exactly once in the interval $(-\infty, 1 - \mu - l)$. In the absence of length parameter and perturbation in the centrifugal force, $x = -\mu$ (Hallan and Rana (2001b)) is the only real root of the Equation 6. By taking into consideration the small perturbation in the centrifugal force, and the length parameter, let the real root of Equation 6 be given by

$$x = -\mu + \epsilon,$$

where ϵ depends on the very small quantities π_2 and l . On putting $x = -\mu + \epsilon$ and $\beta = 1 + \pi_2$ in Equation 6 by restricting ϵ, π_2 up to the linear terms and l up to the second order, we get

$$\epsilon = \frac{\mu(1 + l^2)\pi_2}{(1 + 2\mu) + l^2(1 + 4\mu)}.$$

Therefore, the abscissae of the collinear equilibrium point becomes

$$x = -\mu + \epsilon = -\mu + \nu\pi_2,$$

where

$$\nu = \frac{\mu(1 + l^2)}{(1 + 2\mu) + l^2(1 + 4\mu)}.$$

Thus, the system of Equations (3a)-(3c) has only one collinear equilibrium point $L_1(x, 0, 0)$. It is noticeable that the location of equilibrium point is affected by a small perturbation in the centrifugal force. In the absence of π_2 and l , the equilibrium point L_1 coincides with the center of the shell $(-\mu, 0, 0)$.

Next, we present numerically the effect of perturbations on the location of L_1 . In Table 1, we have represented the numerical values of the abscissas of L_1 for the fixed values of μ and varying values of π_2 and l . It is evident that L_1 lies towards the right or left of the center of the shell according as the perturbation π_2 in the centrifugal force is positive or negative. It can be seen that as we increase the length parameter, L_1 moves along x -axis in its left direction. Also if the small perturbation in centrifugal force is increased, L_1 always lies on the left of x - axis.

Table 1. The abscissae of L_1 for the fixed value of $\mu = 0.001$

l	$\pi_2 = -0.03$	$\pi_2 = -0.02$	$\pi_2 = -0.01$	$\pi_2 = 0.01$	$\pi_2 = 0.02$	$\pi_2 = 0.03$
0.0001	-0.00103086	-0.00102037	-0.10084100	-0.09917400	-0.00098043	-0.00097093
0.1	-0.00103097	-0.00102047	-0.10084700	-0.09918300	-0.00098052	-0.00097103
0.13	-0.00103116	-0.00102066	-0.10086200	-0.09919900	-0.00098071	-0.00097121
0.15	-0.00103138	-0.00102088	-0.10088000	-0.09921800	-0.00098093	-0.00097142
0.17	-0.00103172	-0.00102122	-0.10090600	-0.09924600	-0.00098125	-0.00097174
0.2	-0.00103251	-0.00102200	-0.10096800	-0.09931100	-0.00098200	-0.00097248

Table 2. The abscissae of L_1 for the fixed value of $l = 0.0001$

μ	$\pi_2 = -0.03$	$\pi_2 = -0.02$	$\pi_2 = -0.01$	$\pi_2 = 0.01$	$\pi_2 = 0.02$	$\pi_2 = 0.03$
0.00001	-0.00001031	-0.00001020	-0.00001010	-9.9009×10^{-6}	-9.80393×10^{-6}	-9.70874×10^{-6}
0.00005	-0.00005155	-0.00005102	-0.00005051	-0.00004951	-0.00004902	-0.00004854
0.0001	-0.00010309	-0.00010204	-0.00010101	-0.00009901	-0.00009804	-0.00009709
0.0005	-0.00051545	-0.00051019	-0.00050504	-0.00049505	-0.00049021	-0.00048545
0.001	-0.00103086	-0.00102037	-0.00101008	-0.00099012	-0.00098043	-0.00097093
0.005	-0.00515306	-0.00510101	-0.00505000	-0.00495098	-0.00490291	-0.00485577

The abscissas of L_1 are evaluated for the various values of π_2 , μ and fixed values of $l = 0.0001$ in Table 2. For $\mu = 0.00001$ and $\pi_2 = -0.03$, L_1 lies on the left of the center of m_1 . Further, with the increasing values of $\mu = 0.00001$ to 0.005 , the abscissas of L_1 are becoming smaller, which results L_1 to drift away from the origin.

It is to be noted that Kumar et al. (2019) obtained two out-of-plane equilibrium points for their problem. By out-of-plane equilibrium point, we mean the point lying in (x, z) -plane with $y = 0$. That is, these are the solutions of $W_x = W_y = W_z = 0$ with $x \neq 0$, $y = 0$ and $z \neq 0$. In our problem these points do not exist.

4. The stability of the equilibrium point

We discuss the stability of the equilibrium point in the present section. The motion of the infinitesimal body near the equilibrium point is said to be stable if, when given a very small displacement, the body oscillates for a considerable time around that point. If it departs from the body as the time increases, the motion is unstable.

Consider the equilibrium point $L_1(x, 0, 0)$ and let it be displaced to $(x + \xi, \eta, \zeta)$, where ξ, η, ζ are the small displacements in the x, y, z directions, respectively. Substituting these values in system of Equations (2a)-(2c), we obtain the variational equations

$$\ddot{\xi} - 2\omega\alpha\dot{\eta} = W_{xx}^0\xi + W_{xy}^0\eta + W_{xz}^0\zeta, \quad (7a)$$

$$\ddot{\eta} + 2\omega\alpha\dot{\xi} = W_{yx}^0\xi + W_{yy}^0\eta + W_{yz}^0\zeta, \quad (7b)$$

$$\ddot{\zeta} = W_{zx}^0\xi + W_{zy}^0\eta + W_{zz}^0\zeta, \quad (7c)$$

where the superscript “0” denotes the second order partial derivatives that are evaluated at the equilibrium point under consideration. At the equilibrium point L_1 , rejecting the second and higher powers of π_2 , third and higher powers of l , the second order partial derivatives are

$$W_{xx}^0 = (1 + 2\mu) + \pi_2(1 + 6\mu\tau) + l^2(1 + 4\mu),$$

$$W_{yy}^0 = (1 - \mu) + \pi_2(1 - 3\mu\tau) + l^2(1 - 2\mu),$$

$$W_{zz}^0 = -\mu - 3\mu\tau\pi_2 - 2\mu l^2,$$

$$W_{xy}^0 = W_{yz}^0 = W_{zx}^0 = 0,$$

where $\tau = \mu/(1 + 2\mu)$.

Thus, the system of Equations (7a)-(7c) becomes

$$\ddot{\xi} - 2\omega(1 + \pi_1)\dot{\eta} = (1 + 2\mu + \pi_2(1 + 6\mu\tau) + l^2(1 + 4\mu)) \xi, \tag{8a}$$

$$\ddot{\eta} + 2\omega(1 + \pi_1)\dot{\xi} = (1 - \mu + \pi_2(1 - 3\mu\tau) + l^2(1 - 2\mu)) \eta, \tag{8b}$$

$$\ddot{\zeta} + (\mu + 3\mu\tau\pi_2 + 2\mu l^2) \zeta = 0. \tag{8c}$$

Since $\mu + 3\mu\tau\pi_2 + 2\mu l^2 > 0$ for all the values of the parameters involved, therefore the motion of m_3 parallel to the z -axis is always stable. The characteristic equation corresponding to Equations (8a) and (8b) is a biquadratic equation in λ

$$\lambda^4 + \left(2 - \mu + 8\pi_1 - (2 + 3\tau\mu)\pi_2 + 2(1 - \mu)l^2\right)\lambda^2 + \left((1 + 2\mu)(1 - \mu) + (2 + \mu + 3\mu\tau(1 - 4\mu))\pi_2 + (2 + 3\mu - 8\mu^2)l^2\right) = 0, \tag{9}$$

which admits roots of the form

$$\lambda^2 = \frac{-(2 - \mu + 8\pi_1 - (2 + 3\tau\mu)\pi_2 + 2(1 - \mu)l^2) \pm \sqrt{\Delta}}{2}, \tag{10}$$

where

$$\Delta = \mu(9\mu - 8) + 16(2 - \mu)\pi_1 - 2(8 + 3\tau\mu(4 - 9\mu))\pi_2 + 12\mu(-2 + 3\mu)l^2.$$

In the absence of the length of the finite straight segment m_2 and perturbations in α and β , Δ vanishes when $\mu = 8/9$. However, the solutions in our case will be perturbed. Replacing μ by $\mu^* = 8/9 + \sigma$ ($\sigma \ll 1$) in $\Delta = 0$, we get

$$\sigma = \frac{2}{3} \left(-\frac{10}{3}\pi_1 + \frac{43}{25}\pi_2 - \frac{4}{3}l^2 \right).$$

Hence,

$$\mu^* = \frac{8}{9} + \frac{2}{3} \left(-\frac{10}{3}\pi_1 + \frac{43}{25}\pi_2 - \frac{4}{3}l^2 \right).$$

Table 3. Stability of L_1

Range of μ	λ_1	λ_2	λ_3	λ_4	nature of L_1
$0 < \mu < \mu^*$	$\frac{1}{2}(a + ib)$	$-\frac{1}{2}(a + ib)$	$\frac{1}{2}(a - ib)$	$-\frac{1}{2}(a - ib)$	unstable
$\mu = \mu^*$	ia_1	ia_1	$-ia_1$	$-ia_1$	unstable
$\mu^* < \mu < 1$	ia_2	$-ia_2$	ia_3	$-ia_3$	stable

In Table 3, the nature of L_1 is examined for different ranges of the mass parameter μ . For $0 < \mu \leq \mu^*$, L_1 is unstable and stable for $\mu^* < \mu < 1$. The values of the parameters involved in Table 3 are mentioned in Appendix A.

Consider the surface

$$\Gamma_1(\pi_1, \pi_2, l) = -\frac{10}{3}\pi_1 + \frac{43}{25}\pi_2 - \frac{4}{3}l^2 = 0,$$

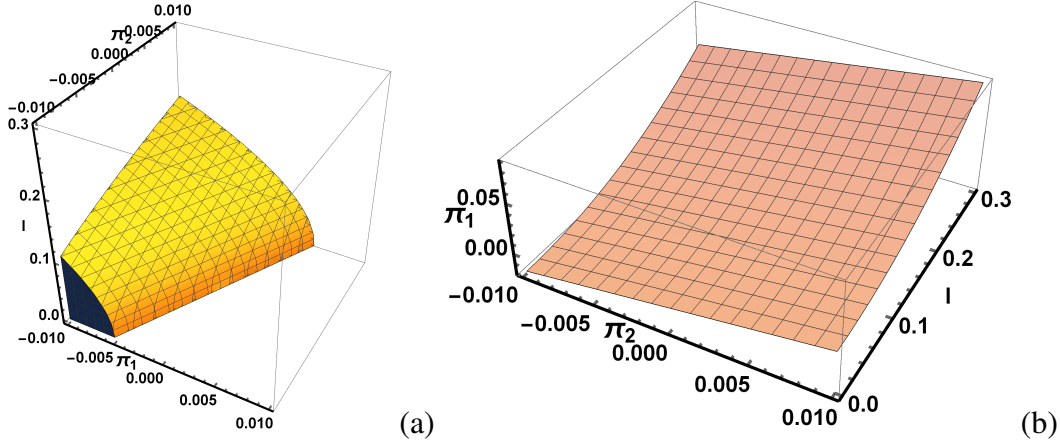


Figure 2. (a) The colored and the non-colored regions represent $\Gamma_1 > 0$ and $\Gamma_1 < 0$, respectively for $-0.01 \leq \pi_1 \leq 0.01$, $-0.01 \leq \pi_2 \leq 0.01$, and $0 \leq l \leq 0.3$. (b) The colored region shows the surface $\Gamma_1 = 0$ when $-0.01 \leq \pi_2 \leq 0.01$, and $0 \leq l \leq 0.3$

which divides the (π_1, π_2, l) -plane into three regions. These regions are shown in Figure 2 for $-0.01 \leq \pi_1 \leq 0.01$, $-0.01 \leq \pi_2 \leq 0.01$ and $0 \leq l \leq 0.3$. The colored and the non-colored regions in Figure 2(a) represents the regions $\Gamma_1 > 0$ and $\Gamma_2 < 0$, respectively. In the region where $\Gamma_1 > 0$, $\mu^* > 8/9$ that clearly shows the decrease in the stability region of L_1 . And in $\Gamma_1 < 0$, $\mu^* < 8/9$ that signifies the increment in the stability region of L_1 . For any point lying on the surface $\Gamma_1 = 0$, as shown by the colored region in Figure 2(b), $\mu^* = 8/9$, that is the range of stability remains unchanged.

Next we consider the (π_1, π_2, l) -plane with no perturbation in the Coriolis force, that is, we take

$$\Gamma_2(0, \pi_2, l) = \frac{43}{25}\pi_2 - \frac{4}{3}l^2 = 0.$$

This divides the $(0, \pi_2, l)$ -plane into different regions that are represented by the different colors as shown in Figure 3 for $0 \leq l \leq 0.20$ and $-0.03 \leq \pi_2 \leq 0.03$. For the region $\Gamma_2 = 0$, we have $\mu^* = 8/9$ that ultimately will not effect the range of stability. It is clear that for $\Gamma_2 > 0$ and $\Gamma_2 < 0$, we have $\mu^* > 8/9$ and $\mu^* < \frac{8}{9}$, respectively. This implies that the range of stability decreases for $\frac{43}{25}\pi_2 - \frac{4}{3}l^2 > 0$ and increases for $\frac{43}{25}\pi_2 - \frac{4}{3}l^2 < 0$ establishing the fact that the centrifugal force is a destabilizing force provided that the Coriolis force is kept constant.

Table 4. The value of μ^* when $\pi_1 = 0$

$l \downarrow \pi_2 \rightarrow$	μ^*					
	-0.03	-0.02	-0.01	0.01	0.02	0.03
0.0001	0.854489	0.865956	0.877422	0.900356	0.911822	0.923289
0.1	0.845600	0.857067	0.868533	0.891467	0.902933	0.914400
0.13	0.839467	0.850933	0.862400	0.885333	0.896800	0.908267
0.15	0.834489	0.845956	0.857422	0.880356	0.891822	0.903289
0.17	0.828800	0.840267	0.851733	0.874667	0.886133	0.897600
0.2	0.818933	0.830400	0.841867	0.864800	0.876267	0.887733

In Table 4, we have calculated the mass parameters μ^* when $\pi_1 = 0$ and for increasing values of π_2 and l . For a fixed $\pi_2 = 0.01$, we observe that as l increases, the range of stability increases.

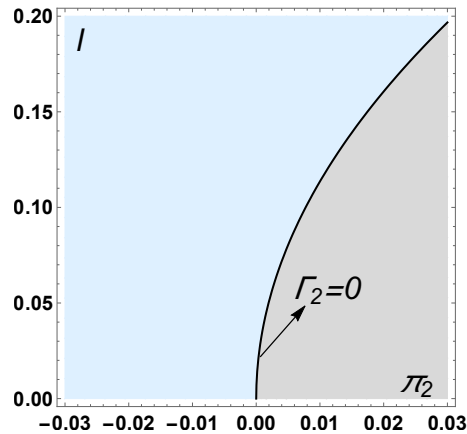


Figure 3. For $0 \leq l \leq 0.20$ and $-0.03 \leq \pi_2 \leq 0.03$, the regions $\Gamma_2 > 0$ and $\Gamma_2 < 0$ are shown by light gray and light blue colors respectively. The region $\Gamma_2 = 0$ is represented by black color

However, on increasing π_2 , the range of stability decreases. For a fixed l , when the centrifugal force is decreased by taking positive values of π_2 , the range of stability increases. When the centrifugal force is increased taking positive values of π_2 , the range of stability decreases.

Similar to Γ_1 and Γ_2 , on taking $\pi_2 = 0$, we have the surface

$$\Gamma_3(\pi_1, 0, l) = -\frac{10}{3}\pi_1 - \frac{4}{3}l^2 = 0.$$

The different regions obtained by $\Gamma_3 = 0$ are shown in Figure 4 by the different colors for $0 \leq l \leq 0.20$ and $-0.03 \leq \pi_1 \leq 0.03$. We have $\mu^* > 8/9$ and $\mu^* < \frac{8}{9}$ when $\Gamma_3 > 0$ and $\Gamma_3 < 0$ respectively. Therefore, the range of stability decreases for $\Gamma_3 > 0$ and increases for $\Gamma_3 < 0$. The range of stability will remain unchanged for all the points lying on the curve $10\pi_1 + 4l^2 = 0$. In Table 5, we have calculated the values of mass parameter μ^* for $\pi_2 = 0$ and increasing values of π_1 and l . We observe that for a fixed $\pi_1 = -0.03$, as l increases the range of stability increases. Also, when $l = 0.0001$, and for the increasing values of π_1 the range of stability increases.

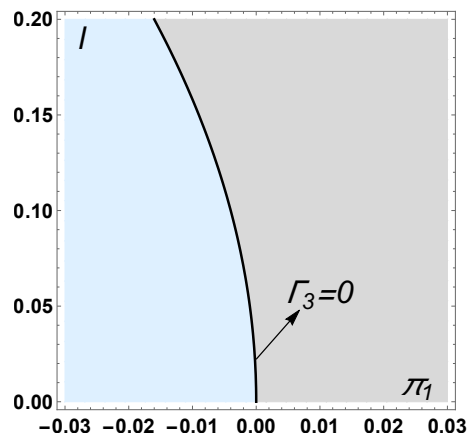


Figure 4. For $0 \leq l \leq 0.20$ and $-0.03 \leq \pi_1 \leq 0.03$, the regions $\Gamma_3 > 0$ and $\Gamma_3 < 0$ are shown by light gray and light blue colors respectively. The region $\Gamma_3 = 0$ is represented by black color

Table 5. The value of μ^* when $\pi_2 = 0$

$l \downarrow \pi_1 \rightarrow$	μ^*					
	-0.03	-0.02	-0.01	0.01	0.02	0.03
0.0001	0.955556	0.933333	0.911111	0.866667	0.844444	0.822222
0.1	0.946667	0.924444	0.902222	0.857778	0.835556	0.813333
0.13	0.940533	0.918311	0.896089	0.851644	0.829422	0.807200
0.15	0.935556	0.913333	0.891111	0.846667	0.824444	0.802222
0.17	0.929867	0.907644	0.885422	0.840978	0.818756	0.796533
0.2	0.920000	0.897778	0.875556	0.831111	0.808889	0.786667

5. Applications

Our model is mathematical whose applicability can be thought as of the motion of submarines in the Earth-Asteroid system. We consider the two primaries m_1^* and m_2 as Earth and asteroid respectively. For the numerical study we gather the data of the different asteroids, namely 216 Kleopatra, 433 Eros, 9 Metis, 22 Kalliope and 4179 Toutatis. The minimum orbit intersection distance (MOID) is chosen as the distance between the primaries. The data for the Earth-Asteroid system is taken from the NASA database (<https://ssd.jpl.nasa.gov/sbdb.cgi>), Lang (1992), and Wikipedia (the free encyclopedia) and given as follows.

• Earth-216 Kleopatra system

Mass of the Earth (m_1^*) = 5.97237×10^{24} kg, mass of the 216 Kleopatra (m_2) = 4.66×10^{18} kg, distance of 216 Kleopatra from the Earth = 1.486 A.U. = 222302436 km and length of the 216 Kleopatra ($2l$) = 276 km. In dimensionless system $m_1^* + m_2 = 1$ unit, that is 5.97237×10^{24} kg = 1 unit. Therefore,

$$\mu = \frac{m_2}{m_1^* + m_2} = 7.80259 \times 10^{-7}.$$

Also, distance between the primaries = 1 unit, that is 222302436 km = 1 unit. Thus, $l = 6.20776 \times 10^{-7}$.

• Earth-433 Eros system

Mass of the 433 Eros (m_2) = 6.69×10^{15} kg, distance of 433 Eros from the Earth = 0.1486 A.U. = 22230243.6 km and length of the 433 Eros ($2l$) = 34.4 km. In dimensionless system $\mu = 1.12016 \times 10^{-9}$ and $l = 7.73721 \times 10^{-7}$.

• Earth-9 Metis system

Mass of the 9 Metis (m_2) = 1.67×10^{19} kg, distance of 9 Metis from the Earth = 1.107 A.U. = 165604843 km and length of the 9 Metis ($2l$) = 245 km. In dimensionless system $\mu = 2.7962 \times 10^{-6}$ and $l = 7.39713 \times 10^{-7}$.

• **Earth-22 Kalliope system**

Mass of the 22 Kalliope (m_2) = 8.42×10^{18} kg, distance of 22 Kalliope from the Earth = 1.638 A.U.= 245041312 km and length of the 22 Kalliope ($2l$) = 215 km. In dimensionless system $\mu = 1.40982 \times 10^{-6}$ and $l = 4.38702 \times 10^{-7}$.

• **Earth-4179 Toutatis system**

Mass of the 4179 Toutatis (m_2) = 5.05×10^{13} kg, distance of 4179 Toutatis from the Earth = 0.006579 A.U.= 984204.391 km and length of the 4179 Toutatis ($2l$) = 4.26 km. In dimensionless system $\mu = 8.4556 \times 10^{-12}$ and $l = 2.16418 \times 10^{-6}$.

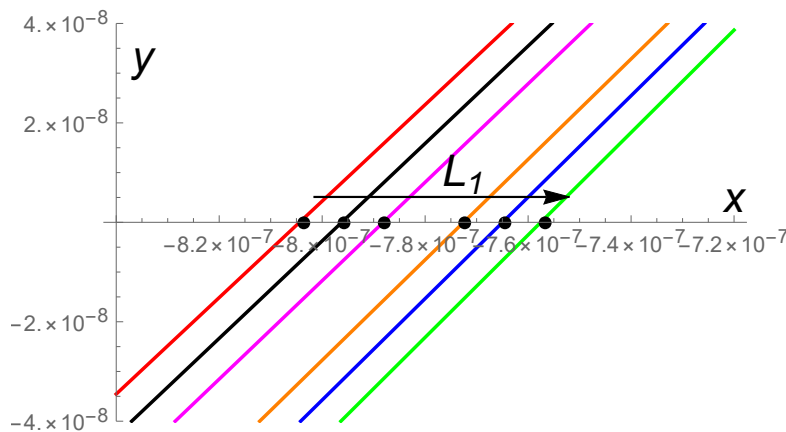


Figure 5. The location of L_1 for the asteroid 216 Kleopatra for different values of $\pi_2 = -0.03$ (red), -0.02 (black), -0.01 (magenta), 0.01 (orange), 0.02 (blue), 0.03 (green)

In Table 6, the locations of equilibrium point L_1 for the different Earth-Asteroid system are represented for the various values of the perturbation in the centrifugal force π_2 . The location of L_1 for 216 Kleopatra asteroid with the different values of π_2 (both positive and negative) is pictorially shown in Figure 5. It is clear that L_1 lies towards the right or left of the center of the shell according as the perturbation π_2 in the centrifugal force is positive or negative. In order to avoid the repetition we have not stated the similar conclusions that are obtained as in the case of other asteroids.

The values of the mass parameter μ^* has been made calculated for the different asteroid for the different values of π_1 and π_2 . This numerical study is categorized in two cases. In the first case, $\pi_2 = 0$ and different values of π_1 are considered and represented in Table 7. The case where $\pi_1 = 0$ with the different values of π_2 are assessed in Table 8.

6. Concluding remarks and discussion

The main objective of our present work is to determine the effect of perturbations π_1 and π_2 in the Coriolis and centrifugal forces in the framework of Robe’s circular restricted three-body prob-

Table 6. The abscissae of L_1 for different asteroids

π_2	216 Kleopatra	433 Eros	9 Metis	22 Kalliope	4179 Toutatis
-0.03	-8.03667×10^{-7}	-1.15376×10^{-9}	-2.88009×10^{-6}	-1.45211×10^{-6}	-8.70927×10^{-12}
-0.02	-7.95864×10^{-7}	-1.14256×10^{-9}	-2.85212×10^{-6}	-1.43802×10^{-6}	-8.62471×10^{-12}
-0.01	-7.88062×10^{-7}	-1.13136×10^{-9}	-2.82416×10^{-6}	-1.42392×10^{-6}	-8.54016×10^{-12}
0.01	-7.72456×10^{-7}	-1.10896×10^{-9}	-2.76824×10^{-6}	-1.39572×10^{-6}	-8.37104×10^{-12}
0.02	-7.64654×10^{-7}	-1.09776×10^{-9}	-2.74028×10^{-6}	-1.38162×10^{-6}	-8.28649×10^{-12}
0.03	-7.56851×10^{-7}	-1.08656×10^{-9}	-2.71231×10^{-6}	-1.36753×10^{-6}	-8.20193×10^{-12}

Table 7. Mass parameter μ^* when $\pi_2 = 0$

Name of the asteroid	l	$\pi_1 = -0.02$	$\pi_1 = -0.01$	$\pi_1 = 0.01$	$\pi_1 = 0.02$
216 Kleopatra	6.20776×10^{-7}	$93333333333.299 \times 10^{-11}$	$91111111111.076 \times 10^{-11}$	$86666666666.632 \times 10^{-11}$	$84444444444.410 \times 10^{-11}$
22 Kalliope	4.38702×10^{-7}	$93333333333.316 \times 10^{-11}$	$91111111111.094 \times 10^{-11}$	$86666666666.649 \times 10^{-11}$	$84444444444.427 \times 10^{-11}$
9 Metis	7.39713×10^{-7}	$93333333333.284 \times 10^{-11}$	$91111111111.062 \times 10^{-11}$	$86666666666.618 \times 10^{-11}$	$84444444444.395 \times 10^{-11}$
433 Eros	7.73721×10^{-7}	$93333333333.280 \times 10^{-11}$	$91111111111.057 \times 10^{-11}$	$86666666666.613 \times 10^{-11}$	$84444444444.391 \times 10^{-11}$
4179 Toutatis	2.16418×10^{-6}	$93333333332.917 \times 10^{-11}$	$91111111110.694 \times 10^{-11}$	$86666666666.250 \times 10^{-11}$	$84444444444.028 \times 10^{-11}$

Table 8. Mass parameter μ^* when $\pi_1 = 0$

Name of the asteroid	l	$\pi_2 = -0.02$	$\pi_2 = -0.01$	$\pi_2 = 0.01$	$\pi_2 = 0.02$
216 Kleopatra	6.20776×10^{-7}	$8659555555.521 \times 10^{-11}$	$8774222222.188 \times 10^{-11}$	$9003555555.521 \times 10^{-11}$	$9118222222.188 \times 10^{-11}$
22 Kalliope	4.38702×10^{-7}	$8659555555.538 \times 10^{-11}$	$8774222222.205 \times 10^{-11}$	$9003555555.538 \times 10^{-11}$	$9118222222.205 \times 10^{-11}$
9 Metis	7.39713×10^{-7}	$8659555555.507 \times 10^{-11}$	$8774222222.174 \times 10^{-11}$	$9003555555.507 \times 10^{-11}$	$9118222222.174 \times 10^{-11}$
433 Eros	7.73721×10^{-7}	$8659555555.502 \times 10^{-11}$	$8774222222.169 \times 10^{-11}$	$9003555555.502 \times 10^{-11}$	$9118222222.169 \times 10^{-11}$
4179 Toutatis	2.16418×10^{-6}	$8659555555.139 \times 10^{-11}$	$8774222221.806 \times 10^{-11}$	$9003555555.139 \times 10^{-11}$	$9118222221.806 \times 10^{-11}$

lem by taking the smaller primary as finite straight segment. In this model, the density ρ_1 of the incompressible fluid within the rigid spherical shell of mass m_1^* is assumed to be same as that of density ρ_3 of m_3 . The system has only one equilibrium point L_1 which is collinear with the center of mass of the primaries. Our results are in accordance with the results obtained by Hallan and Rana (2001a) if the smaller primary is taken to be a point mass instead of a finite straight segment.

The effect of small perturbation in the centrifugal force has a substantial effect on the location of L_1 , but a small perturbation in the Coriolis force has no marked effect on it. In the absence of the perturbations, L_1 coincides with the center of the shell $(-\mu, 0, 0)$. The effects of l and π_2 on the location of the equilibrium point L_1 are also witnessed in Table 1.

It has been concluded that as l increases L_1 lies towards the right or left of the center of the shell according as the perturbation π_2 in the centrifugal force is positive or negative, and moves from right to left along x -axis. Similar behavior of L_1 is observed with the change in the value of mass parameter.

The linear stability of the equilibrium point L_1 is discussed analytically. The range of stability is affected not only by the perturbations in the Coriolis and centrifugal forces but also by the length of the finite straight segment. For $0 < \mu \leq \mu^*$, L_1 is unstable whereas for $\mu^* < \mu < 1$, it becomes stable. The range of stability of L_1 increases or decreases depending on whether the point (π_1, π_2, l) lies in the region $\Gamma_1 < 0$ or $\Gamma_2 > 0$ respectively. The Coriolis force is a stabilizing force provided the centrifugal force is kept constant. We have also investigated the range of stability in the different regions obtained by $\Gamma_2 = 0$ and $\Gamma_3 = 0$ on taking $\pi_1 = 0$ and $\pi_2 = 0$ respectively.

We infer from Table 7 that on increasing π_1 and l , the range of stability increases. Similarly, for a fixed l , the range of stability increases for $\pi_1 > 0$ and decreases for $\pi_1 < 0$. It is also observed that the centrifugal force is a destabilizing force provided the Coriolis force is kept constant. From Table 8, it is clear that for a fixed π_2 , as l increases the range of stability increases. However, on increasing π_2 the range of stability decreases. For a fixed l , when the centrifugal force is decreased by taking the positive values of π_2 , the range of stability increases. On the other hand, the range of stability decreases on increasing the centrifugal force with the positive values of π_2 .

REFERENCES

- Aggarwal, R. and Kaur, B. (2014). Robe's restricted problem of 2+2 bodies with one of the primaries an oblate body, *Astrophys. Space Sci.*, Vol. 352, pp. 467–479.
- Aggarwal, R., Kaur, B. and Yadav, S. (2018). Robe's restricted problem of 2+2 bodies with a Roche ellipsoid-triaxial system, *J. of Astronaut. Sci.*, Vol. 65, No. 1, pp. 63–81.
- Bhatnagar, K.B. and Hallan, P.P. (1978). Effect of perturbations in Coriolis and centrifugal forces on the stability of libration points in the restricted problem, *Celest. Mech. Dyn. Astron.*, Vol. 18, pp. 105–112.
- Chandrashekhar, S. (1987). *Ellipsoidal figures of equilibrium* (Chapter 8). Dover Publication Inc, New York.
- Giordano, C.M., Plastino, A.R. and Plastino, A. (1997). Robe's restricted three-body problem with drag, *Celest. Mech. Dyn. Astr.*, Vol. 66, pp. 229–242.
- Hallan, P.P. and Mangang, K.B. (2008). Effect of perturbations in Coriolis and centrifugal forces on the nonlinear stability of equilibrium point in Robe's restricted circular three-body problem, *Advances in Astron.*, Vol. 55, pp. 512–516.
- Hallan, P.P. and Rana, N. (2001a). Effect of perturbations in Coriolis and centrifugal forces on the location and stability of the equilibrium point in the Robe's circular restricted three-body problem, *Planetary and Space Sci.*, Vol. 49, pp. 957–960.
- Hallan, P.P. and Rana, N. (2001b). The existence and stability of equilibrium points in the Robe's restricted three-body problem, *Celest. Mech. Dyn. Astr.*, Vol. 79, pp. 145–155.

- Jain, R. and Sinha, D. (2014a). Non-linear stability of L_4 in the restricted problem when the primaries are finite straight segments under resonances, *Astrophys. Space Sci.*, Vol. 353, pp. 73–88.
- Jain, R. and Sinha, D. (2014b). Stability and regions of motion in the restricted three-body problem when both the primaries are finite straight segments, *Astrophys. Space Sci.*, Vol. 351, pp. 87–100.
- Kaur, B. and Aggarwal, R. (2012). Robe's problem: Its extension to 2+2 bodies, *Astrophys. Space Sci.*, Vol. 339, pp. 283–294.
- Kaur, B. and Aggarwal, R. (2013a). Robe's restricted problem of 2+2 bodies when the bigger primary is a Roche ellipsoid, *Acta Astronautica*, Vol. 89, pp. 31–37.
- Kaur, B. and Aggarwal, R. (2013b). Robe's restricted problem of 2+2 bodies when the bigger primary is a Roche ellipsoid and the smaller primary is an oblate body, *Astrophys. Space Sci.*, Vol. 349, pp. 57–69.
- Kaur, B., Aggarwal, R. and Yadav, S. (2016). Perturbed Robe's restricted problem of 2+2 bodies when the primaries form a Roche ellipsoid-triaxial system, *J. of Dyn. Systems and Geometric Theories*, Vol. 14, No. 2, pp. 99–117.
- Kumar, D., Kaur, B., Chauhan, S. and Kumar, V. (2019). Robe's restricted three-body problem when one of the primaries is a finite straight segment, *Int. J. of Non-Linear Mech.*, Vol. 109, pp. 182–188.
- Lang, K.R. (1992). *Astrophysical Data: Planets and Stars*, Springer, New York.
- Plastino, A.R. and Plastino, A. (1995). Robe's restricted three-body problem revisited, *Celes. Mech. Dyn. Astron.*, Vol. 61, pp. 197–206.
- Riaguas, A., Elipe, A. and Lopez-Moratalla, T. (2001). Non-linear stability of the equilibria in the gravity field of a finite straight segment, *Celes. Mech. Dyn. Astron.*, Vol. 81, pp. 235–248.
- Robe, H.A.G. (1977). A new kind of three-body problem, *Celes. Mech. Dyn. Astron.*, Vol. 16, pp. 343–351.
- Shrivastava, A.K. and Garain, D. (1991). Effect of perturbation on the location of libration point in the Robe restricted problem of three bodies, *Celest. Mech. Dyn. Astr.*, Vol. 51, pp. 67–73.
- Singh, J. and Leke, O. (2013). Robe's restricted three-body problem with variable masses and perturbing forces, *ISRN Astron. and Astrophys.* 8 pages.
- Singh, J. and Mohammed, H.L. (2012). Robe's circular restricted three-body problem under oblate and triaxial primaries, *Earth, Moon, and Planets*, Vol. 109, pp. 1–11.
- Singh, J. and Mohammed, H.L. (2013). Out-of-plane equilibrium points and their stability in the Robe's problem with oblateness and triaxiality, *Astrophys. Space Sci.*, Vol. 345, pp. 265–271.
- Singh, J. and Omale, A.J. (2014). Robe's circular restricted three-body problem with zonal harmonics, *Astrophys. Space Sci.*, Vol. 353, pp. 89–96.
- Singh, J. and Sandah, A.U. (2012). Existence and linear stability of equilibrium points in the Robe's restricted three-body problem with oblateness, *Advances in Math. Phys.* 18 pages.
- Subbarao, P. and Sharma, R.K. (1975). A note on the stability of the triangular points of equilibrium in the restricted three-body problem, *Astron. Astrophys.*, Vol. 43, pp. 381–383.
- Szebehely, V. (1967). Stability of the points of equilibrium in the restricted problem, *Astron. J.*, Vol. 72, No. 1, pp. 7–9.

Appendix

$$\begin{aligned}
 a &= \sqrt{(\gamma - \delta)}, \quad b = \sqrt{(\gamma + \delta)}, \\
 \delta &= 2 - \mu + 8\pi_1 - (2 + 3\tau\mu)\pi_2 + 2(1 - \mu)l^2, \\
 \gamma &= 2 \left[(1 + 2\mu)(1 - \mu) + (2 + \mu + 3\mu\tau(1 - 4\mu))\pi_2 + (2 + 3\mu - 8\mu^2)l^2 \right]^{1/2}, \\
 a_1 &= \sqrt{\frac{\delta}{2}}, \quad a_2^2 = \frac{1}{2} (\delta - \sqrt{\Delta}), \quad a_3^2 = \frac{1}{2} (\delta + \sqrt{\Delta}).
 \end{aligned}$$